JOURNAL OF MOLECULAR SPECTROSCOPY 160, 422–433 (1993)

Electric Dipole Moments of Rare Gas–Carbonyl Sulfide van der Waals Complexes

ANNE M. ANDREWS,*[,1] LASZLO NEMES,*[,2] SUSAN L. MARUCA,* KURT W. HILLIG II,* ROBERT L. KUCZKOWSKI,* AND JOHN S. MUENTER†

*Department of Chemistry, University of Michigan, Ann Arbor, Michigan 48109-1055; and †Department of Chemistry, University of Rochester, Rochester, New York 14627

The μ_a and μ_b electric dipole moment components of the Ne–OCS, Ar–OCS, and Kr–OCS van der Waals complexes were determined using Fourier transform microwave spectroscopy. The accuracy of these results was evaluated by comparing the Ar–OCS moments with molecular beam electric resonance measurements. The experimental moments are compared with values calculated from projections of the dipole moment of the OCS monomer, corrected for effects from harmonic bending and induced dipole moments in the rare gas atoms. The μ_a and μ_b components were reproduced within 0.01 D for the Ar and Kr complexes and within 0.02–0.025 D for the Ne complex. © 1993 Academic Press, Inc.

INTRODUCTION

High-resolution spectroscopic studies of weakly bound molecular complexes make up an active field of research (*1*) that applies the full arsenal of spectroscopic techniques to the general problem of studying intermolecular potential functions. Pure rotational spectroscopy, primarily using molecular beam electric resonance (*2*) (MBER) or pulsed Fourier transform (*3*) (FTMW) methods, has been particularly productive in this area of research. One reason for this success is the ability of microwave experiments to study complexes in a variety of ways to obtain information on rotational, nuclear hyperfine, electric, and magnetic properties. This paper considers Stark effect measurements and the electric dipole moments of weakly bound complexes in general, and specifically addresses the dipole moments of rare gas–carbonyl sulfide (Rg–OCS) complexes.

In principle, the dipole moment of a bimolecular complex contains a large amount of information. The basic moment arises from the vector sum of the moments of the two monomer constituents and, therefore, contains information about the relative orientation of the monomers within the complex. This basic moment can be significantly modified by dynamic effects associated with large amplitude vibrations and from the polarization of each monomer by the electric fields produced by each binding partner. Thus monomer–monomer vibrational motions and/or molecular charge distortions can be studied through dipole moment measurements if accurate structural data are known. A classic example of using the dipole moment of a complex to study a monomer charge distribution is the determination of the sign of the FCl dipole moment (*4*).

[1] Current address: Molecular Physics Division, National Institute of Standards & Technology, Gaithersburg, MD 20899.

[2] On leave from the Research Laboratory for Inorganic Chemistry, Hungarian Academy of Sciences, Budaorsi ut 45, P.O.B. 132, H-1502 Budapest, Hungary.

0022-2852/93 $5.00

Copyright © 1993 by Academic Press, Inc.
All rights of reproduction in any form reserved.

For these reasons, dipole moment measurements have been a part of high-resolution studies of weakly bound complexes dating from the initial experiments in this area (*5*). Precise dipole moment measurements have traditionally been carried out in MBER experiments. The Fabry–Perot resonator used in FTMW spectrometers makes it more difficult to generate uniform and accurately calibrated Stark fields in these experiments. However, in recent years several FTMW spectrometers have incorporated Stark electrodes and numerous dipole moment measurements have been made with these instruments.

While there has been a relatively large number of dipole moment measurements for weakly bound complexes, methods for interpreting these data are not well developed. The main purpose of this paper is to present measurements of the dipole moment components of Ne–OCS, Ar–OCS, and Kr–OCS. These data are analyzed with a model that uses a harmonic description of large amplitude motions and electric fields from ab initio calculations to calculate polarization effects. A second aspect of this paper is the direct comparison between MBER and FTMW dipole moment measurements to evaluate the accuracy of the latter method.

EXPERIMENTAL DETAILS

The FTMW Stark effect measurements used a Balle–Flygare-type spectrometer at the University of Michigan (*6, 7*). The spectrometer has parallel steel mesh Stark plates, approximately 60 cm square and 30 cm apart, to which potential differences of up to 20 kV can be applied. The electric field was calibrated using the $J = 1, M = 0 \leftarrow J = 0, M = 0$ transition of OCS, with an assumed dipole moment of $\mu = 0.7152$ D (*8*). The absolute accuracy of the field calibration was ±0.3%. The Rg–OCS complexes were prepared by mixing 1% OCS in 99% Ne, Ar, or Kr, using commercial gases without further purification. A stagnation pressure in the range of 1–1.5 atm was used in the pulsed molecular beam source. Transitions were observed under conditions that minimized the Doppler doubling effect that complicates lineshapes (*9*). The observed signals usually did not exhibit any resolved Doppler splitting and had FWHM widths of 20–30 kHz. Measurement uncertainties of the line centers were estimated to be approximately 4 kHz, arising primarily from lineshape variations. The Rg–OCS transitions studied are listed in Table I.

As discussed below, initial FTMW dipole moment results (*10*) for Ar–OCS did not agree well with the original MBER study (*11*) and independent MBER Ar–OCS data were obtained at the University of Rochester. That MBER instrument has been previously described (*12*). In these experiments, a 0.75-atm mixture of 1% OCS in Ar was expanded through a 25-μm diameter nozzle, cooled to dry ice temperature. The cw beam of Ar–OCS was monitored at the parent ion peak, $m/e = 100$, of the mass spectrometer molecular beam detector. Because of the relatively low electric fields used in the Ar–OCS experiments, the Stark field was calibrated using the $J = 2, M = 2 \rightarrow J = 2, M = 2$ radio frequency transition between the *l*-type doublet of the OCS $01^{1}0$ excited vibrational state. The dipole moment of this excited vibrational state is accurately known relative to the OCS ground state (*13*), and the zero field frequency and Stark coefficient for this transition are similar to those of the Ar–OCS transitions studied. The FWHM linewidths for the transitions were 1–2 kHz and signal to noise ratios were sufficient to achieve measurement uncertainties of ±100 Hz. The absolute accuracies of the dipole moments reported here are 0.03%. The $2_{20}, M = 2 \rightarrow 2_{21}, M = 2$ and the $2_{02}, M = 0 \rightarrow 1_{11}, M = 0$ Ar–OCS transitions were studied, with results given in Table II.

TABLE I

Stark Effect Data for Rg–OCS Complexes from FTMW Spectroscopy

	$J_{K_aK_c} \leftarrow J_{K_aK_c}$	M [a]	$\Delta\nu/E^2$ [b] (obs.)	$\Delta\nu/E^2$ (obs.) − $\Delta\nu/E^2$ [c] (calc.)
Ne–OCS				
	$1_{11} \leftarrow 0_{00}$	0	5.76(5)	−0.037
	$2_{12} \leftarrow 1_{01}$	1	5.57(8)	0.108
	$2_{02} \leftarrow 1_{01}$	0	1.52(2)	−0.012
	$2_{02} \leftarrow 1_{01}$	1	5.67(10)	−0.082
	$2_{12} \leftarrow 1_{11}$	1	11.71(8)	−0.009
	$2_{11} \leftarrow 1_{10}$	0	1.04(5)	0.012
	$2_{11} \leftarrow 1_{10}$	1	−12.48(4)	−0.017
Ar–OCS				
	$4_{04} \leftarrow 3_{03}$	0	−1.28(2)	−0.007
	$4_{04} \leftarrow 3_{03}$	1	−0.695(9)	0.000
	$4_{04} \leftarrow 3_{03}$	2	1.03(2)	0.006
	$4_{04} \leftarrow 3_{03}$	3	3.88(2)	−0.010
	$2_{12} \leftarrow 1_{01}$	0	−0.489(7)	0.000
	$2_{12} \leftarrow 1_{01}$	1	4.58(3)	0.005
Kr–OCS				
	$1_{11} \leftarrow 0_{00}$	0	14.13(3)	0.000
	$3_{13} \leftarrow 2_{02}$	0	1.025(6)	−0.003
	$3_{13} \leftarrow 2_{02}$	1	1.532(7)	0.003
	$3_{13} \leftarrow 2_{02}$	2	3.03(4)	0.000

a. M value for parallel, $\Delta M=0$, transitions.

b. $\Delta\nu$ in MHz, E in kv/cm.

c. Calculated using FTMW values for μ_a and μ_b from Table III.

DIPOLE MOMENT MEASUREMENTS

The Rg–OCS complexes are necessarily planar, with the c-inertial axis perpendicular to the molecular plane. Thus there are two nonvanishing components of the dipole moment, μ_a and μ_b, which must be extracted from the observed Stark effect data. For the FTMW data, all relevant zero field energy level spacings were very much larger than the field-induced energy level shifts, and second-order perturbation theory is quite adequate to analyze the data (*14*). In this situation, plots of $\Delta\nu$ vs E^2 are linear and exhibit second-order Stark coefficients that depend on μ_a, μ_b and the rotational constants. The data for a given transition were first least-squares fit to a second-order Stark coefficient and the results of these fits are listed in column 3 of Table I. Using the rotational constants of Ref. (*9*), these coefficients were then least-squares fit by adjusting the dipole moment components. The dipole moments obtained in this way are listed in Table III. These moments, and the rotational constants, were then used to calculate second-order Stark coefficients, which are compared with the observed values in the last column of Table I. Ne–OCS and Kr–OCS Stark effects have not previously been studied.

TABLE II

MBER Stark Effect Data for the Ar–OCS Complex

$J_{K_aK_c} \rightarrow J_{K_aK_c}$	M[a]	E/(V/cm)	ν/(MHz)
$2_{20} \rightarrow 2_{21}$	2	0.000	11.05415(10)
	2	29.966	11.86383(10)
$2_{02} \rightarrow 1_{11}$	0	0.000	186.09125(10)
	0	99.909	186.91310(10)

a. M value for parallel, $\Delta M=0$, transitions.

The MBER data were analyzed somewhat differently. The two transitions studied were selected because the Stark effect for the 2_{20}, $M = 2 \rightarrow 2_{21}$, $M = 2$ transition depends only on μ_a, to within a few parts in 10^5, while the 2_{02}, $M = 0 \rightarrow 1_{11}$, $M = 0$ Stark effect is dominated by μ_b. Two-level perturbation theory (*14*) was used to obtain μ_a from the $2_{20} \rightarrow 2_{21}$ frequency shift. About 3% of the 2_{02}, $M = 0 \rightarrow 1_{11}$, $M = 0$ Stark effect depends on μ_a, with the remaining 97% arising from a single two-level interaction involving μ_b. The μ_a result from the $2_{20} \rightarrow 2_{21}$ transition permits an accurate value of μ_b to be obtained from the $2_{02} \rightarrow 1_{11}$ data. The moments obtained in this way are in excellent agreement with the original study of Ar–OCS (*11*), and both sets of MBER results are listed in Table III.

The initial values for dipole moment components obtained from the FTMW data were somewhat different from those reported in Table III (*10*). In particular, these early FTMW results for Ar–OCS differed from the original MBER dipole moments (*11*) by a small but significant amount (0.005 D for μ_a and 0.012 D for μ_b). It was at this stage that the University of Rochester work was initiated, and independent MBER data agreed with the Harvard results. Reevaluation of the FTMW data brought to light some small problems that combined to produce dipole moments with errors larger than the statistical uncertainties had indicated. The problems related to non-uniform lineshapes, small frequency shifts for some transitions, and calibration procedures. The general question of uncertainties obtained from FTMW instruments is addressed in more detail under the Discussion. In view of the difficulty of making high-accuracy FTMW Stark effect measurements, the FTMW results in Table III have quoted uncertainties substantially larger than would be obtained from the standard deviations of the least-squares fit. This conservative approach to estimating possible errors leads to rather large uncertainties in μ_b for Ne–OCS and μ_a for Kr–OCS.

ANALYSIS

The Rg–OCS dipole moments, μ_T, in Table III are all less than the OCS monomer moment (0.715 D) and the moments become progressively smaller as the size of the rare gas atom increases. This observation can be explained qualitatively as arising from induced dipole moments in the Rg atoms generated by electric fields produced by the OCS charge distribution. In a T-shaped complex, this induced moment will

TABLE III

Experimental Dipole Moments, in Debye, for Rg–OCS Complexes[a]

		Ne–OCS	Ar–OCS	Kr–OCS
FTMW (current)				
	μ_a	0.329(4)	0.214(6)	0.172(10)
	μ_b	0.626(15)	0.666(2)	0.675(3)
	μ_T	0.707(13)	0.700(3)	0.696(4)
MBER (current)				
	μ_a		0.21423(6)	
	μ_b		0.6668(2)	
	μ_T		0.7004(2)	
MBER (ref. 11)				
	μ_a		0.2146(10)	
	μ_b		0.669(2)	
	μ_T		0.7026(20)	

a. μ_T is the vector sum of μ_a and μ_b. See text for a discussion of the uncertainties.

subtract from the monomer permanent moment, while the induced and permanent moments would add in a linear complex. The Rg–OCS complexes are roughly T-shaped and the Ne-Ar-Kr trend is accounted for by the increasing polarizability of the Rg atoms with increasing size. Since the Rg–OCS complexes are only approximately T-shaped, it is necessary to focus on the individual μ_a and μ_b components. It is also necessary to consider how these components are affected by large amplitude vibrational motions.

The angles needed to project the OCS moment onto the principal inertial axes are defined in Fig. 1. The geometry of the complex is determined by R, the distance from the OCS center of mass (com) to the Rg atom, and the angle θ between the OCS axis and R. θ is defined as the O-com-Rg angle. χ is the angle between the a-inertial axis and R. While we would like to know θ_{eq}, the equilibrium value of θ, the experimentally determined (*9*) effective value for this angle, θ_{eff}, is a close approximation for θ_{eq}. Table IV lists θ_{eff} and χ values for the three Rg–OCS molecules considered here (*9*). Table V lists the experimental and several different calculated values for the Rg–OCS dipole moment components. The first calculated set of moments, labeled *projection*, contains the results for projecting the OCS monomer moment on the a- and b-axes. The agreement between the observed and projected μ_b values is quite good. However, the μ_a components exceed the measurements by 10 to 30%.

The next step is to consider the effects of averaging the projections of the monomer moment over the zero point amplitude of the van der Waals bending vibration. This problem was discussed for Ar–OCS in the original publication (*11*) and has been

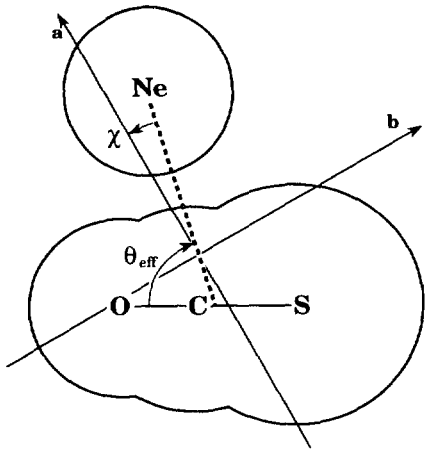

FIG. 1. Principal axis system for Ne–OCS showing definitions of χ, the angle between the a-axis and R, and θ_{eff}, the angle between the OCS-axis and R, where R intersects OCS at its center of mass.

further developed by Novick (*15*). Novick begins with a harmonic oscillator description of the zero point bending motion, using a $v = 0$ wavefunction of

$$\psi_0(\theta) = N \cdot \exp[(-\alpha/2)(\theta - \theta_{eq})^2], \tag{1}$$

where

$$\alpha = 2\pi\mu_r\nu_b/\hbar = \mu_r\omega_b/\hbar = (\mu_r k)^{1/2}/\hbar. \tag{2}$$

In Eq. (1), N is the normalization constant and the coefficient α in the exponent depends on the reduced mass μ_r, the bending frequency ν_b (or the angular frequency ω_b), or the force constant k. The units for the reduced mass are those of a moment

TABLE IV

Structural and Vibrational Parameters for Rg–OCS Complexes[a]

	Ne–OCS	Ar–OCS	Kr–OCS
χ	11.6°	5.3°	3.2°
θ_{eff}	70.4°	73.0°	74.1°
μ_r/amu·Å^2	32.35	36.36	37.36
ν_b/cm^{-1}	15.5[b]	26.0[c]	26.1[b]

a. The values used for χ and θ_{eff} are from ref. 9; see Fig. 1 for the definition of these angles. μ_r and ν_b are the reduced mass and vibrational frequency for the harmonic bender model.

b. Calculated from the inertial defect, see ref. 18.

c. From ref. 17b.

TABLE V

Observed and Calculated Values for Rg–OCS Dipole Moments

	Ne–OCS/(D)	Ar–OCS/(D)	Kr–OCS/(D)
experimental			
μ_a	0.329	0.214	0.172
μ_b	0.626	0.666	0.675
projection			
μ_a	0.370	0.265	0.223
μ_b	0.612	0.664	0.680
harmonic bender			
μ_a	0.364	0.266	0.229
μ_b	0.602	0.657	0.671
harmonic bender + polarization			
μ_a	0.350	0.216	0.163
μ_b	0.602	0.659	0.676
harmonic bender + polarization − experimental			
μ_a	0.021	0.002	−0.009
μ_b	−0.024	−0.007	0.001

of inertia, mass × distance^2, and k has energy units. Finally, θ_{eff} will be used rather than θ_{eq}. Expectation values from Ref. (*15*) give

$$\langle 0|\mu_{\parallel}|0\rangle = \cos(\theta_{\text{eff}}) \cdot \mu_{\text{OCS}} \cdot \exp[-1/(4\alpha)], \tag{3}$$

$$\langle 0|\mu_{\perp}|0\rangle = \sin(\theta_{\text{eff}}) \cdot \mu_{\text{OCS}} \cdot \exp[-1/(4\alpha)]. \tag{4}$$

The $\parallel$ and $\perp$ subscripts in Eqs. (3) and (4) refer to the moment components parallel and perpendicular to R, from which μ_a and μ_b can be obtained. The reduced mass, μ_r, was approximated as the inverse of the diagonal $G_{\theta\theta}$ matrix element from a normal mode analysis (*16*), and the values used are listed in Table IV. The bending frequencies, v_b, can be obtained either from an analysis of centrifugal distortion constants (*17*) or from the inertial defect (*18*, Eq. c). For each of the three complexes, the two methods gave v_b's that agreed to within 5%. The values used to implement Eqs. (3) and (4) are listed in Table IV.

Using this procedure to calculate $\mu_{\parallel}$ and $\mu_{\perp}$, which were rotated to give the μ_a and μ_b listed in Table V as the *harmonic bender* results, produces results that are very similar to the simpler *projection* moment components. The only significant changes are for Ne–OCS, which is not surprising since it has the smallest reduced mass and

bending force constants. The largest change introduced by the vibrational averaging calculation occurs for μ_b of Ne–OCS, and this 0.01 D change takes the calculated moment farther from the observed value. Since the dipole moment corrections associated with the bending vibration are generally quite small, the assumptions made in deriving and applying Eqs. (3) and (4) are not likely to have any significant effect on the calculated moment components.

This leaves induction effects as the major source of the differences between calculated and observed dipole moment components. There are several possible approaches to this issue. Since the polarizabilities of the Rg atoms are known (*19*), the problem is apparently reduced to finding the electric field vector at the Rg location. This can be done using a multipole expansion of the OCS charge distribution (*20*), but slow convergence of the multipole expansion at van der Waals molecule distances and the limited number of available multipole moments make this approach difficult to implement. Specific examples of this convergence problem have been discussed for the cases of Ar–furan and Ar–pyrrole (*21*). A second approach, and the one used here, is to obtain the electric fields from an ab initio quantum chemistry calculation. Finally, one could calculate the field produced by OCS from a distributed multipole description of the OCS charge distribution (*22*).

The GAUSSIAN 86 quantum chemistry package (*23*) was used to calculate an OCS wavefunction, using the 6-311G* basis set. The ability of the calculation to give proper electric fields can be judged, in part, from the calculated OCS dipole moment, μ_{OCS} = 0.62 D, which is 13% lower than the observed value. The ab initio E field calculation was done in an OCS-based coordinate system and then the field components parallel and perpendicular to the OCS axis were rotated into the inertial axis systems of the complexes. The electric field generated by the OCS charge distribution is shown qualitatively in Fig. 2; note the rapid spatial variation of both the magnitude and the

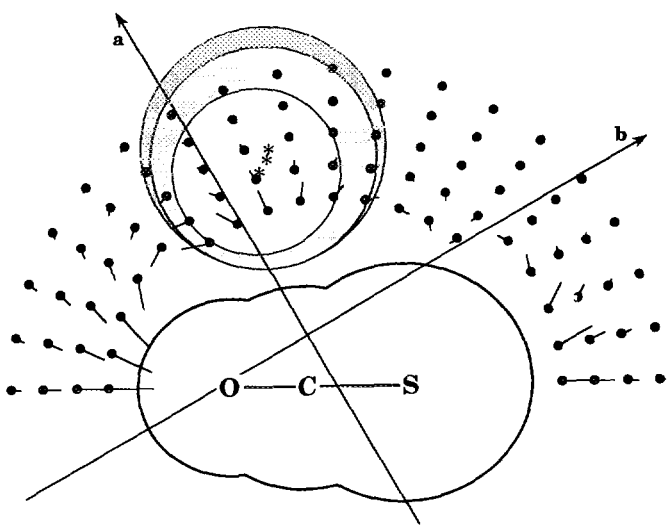

FIG. 2. The principal inertial axis system is for Ne–OCS with nuclear centers and van der Waals radii indicated for Ne, Ar, and Kr. The positive a and b directions indicated by the arrows are chosen to correspond to the positive direction for the projected dipole components for OCS. The electric field lines are plotted on a grid in one hemisphere about OCS with the tail illustrating the relative magnitude and the direction of the field lines. The more positive region is at the end embedded in the grid point.

direction of the field. Figure 2 also shows the locations of the three different Rg atoms. The *a* and *b* components of the field at each of these three points are listed in Table VI and these were used to calculate induced dipole moment components, treating the Rg atom as having a point polarizability (*19*). The resulting induced moment components are included in Table VI. These induced moments are combined with the *harmonic bender* results in Table V to give the *harmonic bender + polarization* calculations in Table V. The final numbers in Table V are calculated minus observed residuals, i.e., the *harmonic bender + polarization* moments minus the *experimental* moments.

If we realistically set our expectations for success at the ±0.01 D level, the *harmonic bender + polarization* results are quite good for Ar–OCS and Kr–OCS. The calculated Ne–OCS components are less satisfactory, differing from the observed moments by more than 0.02 D. However, the experimental uncertainties are also relatively large for Ne–OCS, with the possible error in μ_b larger than 0.01 D. All of these results are addressed in greater detail under the Discussion.

DISCUSSION

We wish to discuss two separate aspects of the work presented here. First, some general comments are made on the accuracy of dipole moments of weakly bound complexes measured with FTMW spectroscopy. Then we discuss some specific details of the Rg–OCS results.

The characteristics of the Fabry–Perot resonator used in FTMW spectrometers place a number of constraints on the electric field used for Stark effect measurements. The maximum field strength available is on the order of 1000 V/cm and limitations on the dimensions and separation of the Stark electrodes means that the field cannot be extremely uniform. This latter property places special demands on the calibration process. The most common operating mode for an FTMW instrument has the molecular beam propagating perpendicularly to the Fabry–Perot axis, and in this configuration the FWHM linewidth can vary between 10 and 30 kHz. Frequency shifts from the Stark effect can be measured to a small fraction of a linewidth only when low noise data exhibiting very stable lineshapes are available. The lineshape is a subtle function of beam source conditions, pulse timings, and electric field inhomogeneities. Lineshapes can vary substantially, even for a single Stark component of a specific

TABLE VI

Electric Field Components and Induced Dipole Moments in the Rg Atom of Rg–OCS Complexes[a]

	Ne–OCS	Ar–OCS	Kr–OCS
$E_a/10^6$ v/cm	11.1	8.66	7.50
$E_b/10^6$ v/cm	0.25	0.58	0.65
μ_a(induced) D	−0.014	−0.050	−0.066
μ_b(induced) D	0.000	0.002	0.005

a. A negative sign for an induced moment component implies a negative to positive direction opposite to the sign of the internal axis system shown in Fig. 2.

transition. These problems translate to Stark effect measurement precisions of 1–5 kHz. Because of the modest intensity and homogeneity of the field, useful Stark shifts are typically on the order of 1 MHz and many transitions will not allow frequency shifts this large. These considerations mean that it is quite difficult to achieve Stark coefficient precisions of better than 0.1%, and in less than optimum cases the precision may be less than 1%.

A consistent calibration procedure is essential to convert this precision to an accuracy. It is important that the calibrant and sample molecules occupy the same volume element of the field. In FTMW experiments, this is only true when the calibrant and sample transitions have similar frequencies and when the calibration lineshape is identical to the van der Waals molecule lineshape. Because widely different source conditions are often employed for the measurement and calibration, this is frequently not the case. It is particularly important that the transitions used for both calibration and measurement exhibit symmetric lineshapes. These considerations lead to the possible presence of unknown systematic errors in Stark effect data.

The problems discussed here were encountered to a small degree in the initial FTMW Rg–OCS measurements (*10*) carried out for this work, and substantial care was required to minimize their influence on the final results. All of this discussion can be summarized by noting that FTMW measurements can yield dipole moments of 1% accuracy relatively easily, but 0.1% accuracy is quite difficult to achieve. Fortunately, much of the information residing in the dipole moments of weakly bound complexes is available at the 1% level of accuracy.

The remaining discussion relates to the results given in Table V. The most obvious point of concern is the relatively poor agreement between the calculated and observed Ne–OCS dipole moment components. Since Ne–OCS is the most "floppy" of the three complexes, it is natural to consider vibrational averaging as the origin of the problem. However, vibrational averaging problems could reside in both the polarization contribution and inadequacies in the harmonic bender model used. In addition, μ_b for Ne–OCS has a large experimental uncertainty. So it is not possible to attribute problems with Ne–OCS to any single cause. Instead, some general comments on the dipole moment calculations are made.

The possible inadequacies of the harmonic bender model used for vibrational averaging can arise both from the harmonic approximation and from assuming a pure bending motion. The treatment used here (*15*) considered the length of the R vector to be independent of the angle θ, which need not be the case. For example, a plausible description of a Rg–OCS complex might be a spherical atom interacting with a cylindrical linear molecule. This kind of approach has been used to model the carbon dioxide dimer (*24*). A reasonable low-frequency vibration in this model could have the Rg atom translating back and forth along the molecule, a motion that cannot be described as a simple bend. The dipole moment effects introduced by anharmonicities and stretch–bend interactions will be small for relatively rigid complexes, but can certainly be substantial for a molecule like Ne–OCS. Obviously, questions concerning anharmonicities and stretch–bend interactions cannot be addressed quantitatively without detailed information on the intermolecular potential function of the complex in question.

A second question on vibrational averaging arises when induced dipole moment components are considered. As shown in Fig. 2, both the magnitude and the orientation of the electric field generated by the OCS charge distribution varies rapidly as a function of the rare gas atom position. This means that large amplitude motions of the Rg

atom can affect the size of the induced dipole moment and also change how that moment is distributed between μ_a and μ_b. Fortunately, for the present work, the largest amplitude motions occur in Ne–OCS where the induced moments are the smallest. Because the more polarizable Rg atoms exhibit smaller amplitude motions than those found in Ne–OCS, vibrational averaging effects on the induced moments are probably not too significant for the Rg–OCS complexes.

An assumption made in the calculations of dipole moments induced in the Rg atoms, which is probably more serious than omitting vibrational averaging over the polarizing field, was assigning the atom a point polarizability. Figure 2 clearly shows that the magnitude and direction of the OCS-derived electric field change enormously over the volume occupied by the Rg atom. A distributed polarizability approach which deals with this problem has been developed by Stone and co-workers (*25*). The distributed polarizability calculation requires the potential, the field, and the field gradient at the location of the Rg atom. In the Ar–OCS and Kr–OCS cases, relatively good results are obtained from the simpler calculation, presumably because of canceling errors. This was also true for the Ar–furan and Ar–pyrrole complexes (*21*). However, this cancellation of errors need not be a general phenomenon.

SUMMARY AND CONCLUSIONS

Dipole moment measurements have been made on Ne–OCS, Ar–OCS, and Kr–OCS using a Fourier transform microwave spectrometer. Independent molecular beam electric resonance measurements of the Ar–OCS Stark effect were made to evaluate the accuracy of FTMW Stark data. The Rg–OCS dipole moments were analyzed by projecting the monomer moment onto the inertial axes of the complexes, using a harmonic bender model. These results were then corrected for induced moments arising from polarization of the Rg atoms. This procedure successfully described the dipole moment components of Ar–OCS and Kr–OCS, but was less successful for Ne–OCS. The approximations and limitations of these calculations are discussed, as are the capabilities of FTMW dipole moment measurements.

ACKNOWLEDGMENTS

The work at Michigan and Rochester was supported by grants from the Experimental Physical Chemistry Program, National Science Foundation, Washington DC. S.L.M. acknowledges fellowship support from the Summer Undergraduate Research Program of the University of Michigan Chemistry Department. A.M.A. was the recipient of a Regents Graduate Fellowship from the University of Michigan. We are grateful to Dr. Amine Taleb-Bendiab for help in calculating vibrational frequencies.

RECEIVED: December 29, 1992

REFERENCES

1. S. E. NOVICK, "Bibliography of Rotational Spectra of Weakly Bound Complexes," Dept. of Chemistry, Wesleyan University, Middletown, CT, 1991; S. E. NOVICK, K. R. LEOPOLD, AND W. A. KLEMPERER, *in* "Atomic and Molecular Clusters" (E. R. Bernstein, Ed.), Chap. 3, pp. 359–392, Elsevier, Amsterdam, 1990.
2. J. S. MUENTER, "Electric and Magnetic Resonance Spectroscopy, Atomic and Molecular Beam Methods" (G. Scoles, Ed.), Vol. II, Ch. 2, pp. 15–57, Oxford Univ. Press, London, 1992.
3. A. C. LEGON, *Annu. Rev. Phys. Chem.* **34**, 275–300 (1983).
4. S. E. NOVICK, K. C. JANDA, AND W. A. KLEMPERER, *J. Chem. Phys.* **65**, 5115–5121 (1976).
5. T. R. DYKE, B. J. HOWARD, AND W. A. KLEMPERER, *J. Chem. Phys.* **56**, 2442–2454 (1972).
6. T. J. BALLE AND W. H. FLYGARE, *Rev. Sci. Instrum.* **52**, 33–45 (1981).

7. K. W. HILLIG, II, J. MATOS, A. SCIOLY, AND R. L. KUCZKOWSKI, *Chem. Phys. Lett.* **133,** 359–362 (1987).
8. J. S. MUENTER, *J. Chem. Phys.* **48,** 4544–4547 (1968); F. DE LEEUW AND A. DYMANUS, *Chem. Phys. Lett.* **7,** 288–292 (1970); K. TANAKA, H. ITO, K. HARADA, AND T. TANAKA, *J. Chem. Phys.* **80,** 5893–5905 (1984).
9. F. J. LOVAS AND R. D. SUENRAM, *J. Chem. Phys.* **87,** 2010–2020 (1987).
10. L. NEMES, S. L. MARUCA, A. M. ANDREWS, K. W. HILLIG, II, The Ohio State Univ. International Symposium on Molecular Spectroscopy, paper FA7, 1991.
11. S. J. HARRIS, K. C. JANDA, S. E. NOVICK, AND W. KLEMPERER, *J. Chem. Phys.* **63,** 881–884 (1975).
12. B. FABRICANT, D. KREIGER, AND J. S. MUENTER, *J. Chem. Phys.* **67,** 1576–1586 (1977).
13. J. M. L. J. REINARTZ, W. L. MEERTS, AND A. DYMANUS, *Chem. Phys. Lett.* **16,** 576–580 (1972).
14. W. GORDY AND R. L. COOK, "Microwave Molecular Spectra," 3rd ed., Wiley, New York, 1984.
15. S. E. NOVICK, *J. Mol. Spectrosc.* **118,** 550–552 (1986).
16. E. B. WILSON, Jr., J. C. DECIUS, AND P. A. CROSS, "Molecular Vibrations," McGraw–Hill, New York, 1955.
17. J. M. STEED, T. A. DIXON, AND W. A. KLEMPERER, *J. Chem. Phys.* **70,** 4095–4100 (1979); J. A. SHEA, W. G. READ, AND E. J. CAMPBELL, *J. Chem. Phys.* **79,** 2559–2568 (1983).
18. D. R. HERSCHBACH AND V. W. LAURIE, *J. Chem. Phys.* **40,** 3142–3153 (1964).
19. R. H. ORCUTT AND R. H. COLE, *J. Chem. Phys.* **46,** 697–702 (1967).
20. C. H. JOYNER, T. A. DIXON, F. A. BAIOCCHI, AND W. KLEMPERER, *J. Chem. Phys.* **75,** 5285–5290 (1981).
21. R. K. BOHN, K. W. HILLIG, II, AND R. L. KUCZKOWSKI, *J. Phys. Chem.* **93,** 3456–3459 (1989); J.-J. OH, K. W. HILLIG, II, R. L. KUCZKOWSKI, AND R. K. BOHN, *J. Phys. Chem.* **94,** 4453–4455 (1990).
22. A. J. STONE, *Chem. Phys. Lett.* **83,** 233–239 (1981); A. D. BUCKINGHAM AND P. W. FOWLER, *Can. J. Chem.* **63,** 2018–2025 (1985); G. J. B. HURST, P. W. FOWLER, A. J. STONE, AND A. D. BUCKINGHAM, *Int. J. Quantum Chem.* **29,** 1223–1239 (1986).
23. J. M. FRISCH, J. S. BINKLEY, H. B. SCHLEGEL, K. RAGHAVACHAN, C. F. MELIUS, R. L. MARTIN, J. J. P. STEWART, F. W. BOBROWICZ, C. M. ROHLFING, L. R. KAHN, D. J. DEFREES, R. A. WHITESIDES, D. J. FOX, E. M. FLUDER, AND J. A. POPLE, "GAUSSIAN 86," Carnegie-Mellon Quantum Chemistry Publishing Unit, Pittsburgh, PA, 1986.
24. M. A. WALSH, T. H. ENGLAND, T. R. DYKE, AND B. J. HOWARD, *Chem. Phys. Lett.* **142,** 265–270 (1987).
25. A. J. STONE, *Mol. Phys.* **56,** 1065–1082 (1985); P. W. FOWLER, A. J. STONE, AND A. D. BUCKINGHAM, *Int. Rev. Phys. Chem.* **5,** 107–114 (1986); P. W. FOWLER AND A. J. STONE, *J. Phys. Chem.* **91,** 509–511 (1987); C. R. LESUEUR, A. J. STONE, AND P. W. FOWLER, *J. Phys. Chem.* **95,** 3519–3522 (1991).